MOCVD homoepitaxy of Si-doped (010) β -Ga₂O₃ thin films with superior transport properties

Zixuan Feng, 1,a) A F M Anhar Uddin Bhuiyan, 1 Md Rezaul Karim, 1 and Hongping Zhao 1,2,b)

Record-high electron mobilities were achieved for silicon-doped (010) β-Ga₂O₃ homoepitaxial films grown via metalorganic chemical vapor deposition (MOCVD). Key growth parameters were investigated to reduce the background doping and compensation concentration. Controllable n-type Si doping was achieved as low as low-10¹⁶ cm⁻³. Record carrier mobilities of 184 cm²/V·s at room temperature and 4984 cm²/V·s at low temperature (45 K) were measured for β-Ga₂O₃ thin films with room-temperature doping concentrations of 2.5×10¹⁶ and 2.75×10¹⁶ cm⁻³, respectively. Analysis of temperature-dependent Hall mobility and carrier concentration data revealed a low compensation concentration of 9.4×10¹⁴ cm⁻³. Using the two-donor model, Si on the tetrahedrally coordinated Ga(I) site represented the primary shallow donor state, and the secondary donor state was found to possess an activation energy of 120 meV. The demonstration of high-purity and high-quality β-Ga₂O₃ thin films with uniform and smooth surface morphology via MOCVD will harness its advantages as an ultrawide-bandgap semiconductor for power electronic and short-wavelength optoelectronic device applications.

Keywords: Ultrawide bandgap, β -Ga₂O₃ thin films, homoepitaxy, Si doping, metalorganic chemical vapor deposition

¹Department of Electrical and Computer Engineering, The Ohio State University, Columbus, OH 43210, USA

²Department of Materials Science and Engineering, The Ohio State University, Columbus, OH 43210, USA

^{a)}E-mail: feng.890@osu.edu; ^{b)}Corresponding author E-mail: zhao.2592@osu.edu

Thermally stable β-Ga₂O₃ possesses an ultrawide bandgap of 4.5–4.9 eV,^{1,2} which holds great promise for applications in power electronic devices³ and solar-blind ultraviolet photodetection.⁴ The theoretically predicted critical field³ of 6–8 MV/cm and room-temperature electron mobility of 200-300 cm²/V·s lead to a two- to threefold higher Baliga's figure of merit⁵ for β-Ga₂O₃ compared to traditional wide-bandgap semiconductors such as SiC and GaN. One key advantage of β-Ga₂O₃ is the availability of high-quality and scalable native substrates synthesized via melt growth techniques, such as the floating zone method, 6-9 Czochralski method, 10-12 and edge-defined film-fed growth method. 13,14 Irrespective of its early stage development, β-Ga₂O₃-based Schottky barrier diodes with a breakdown voltage of 2.3 kV¹⁵ and lateral field-effect transistors with a breakdown voltage of 755 V and channel current of 100 mA/mm¹⁶ have been realized. Recently, the use of modulation-doped β-(Al_xGa_{1-x})₂O₃/Ga₂O₃ heterostructures to form a two-dimensional electron gas with a room-temperature channel mobility of 180 cm²/V·s and sheet charge density of 2×10¹² cm⁻² was demonstrated.¹⁷ These preliminary devices indicate the great potential of β-Ga₂O₃ as an enabling ultrawide-bandgap semiconductor for advancing device technologies in power electronics and short-wavelength optoelectronics.

Single-crystal β -Ga₂O₃ thin-film epitaxy has been investigated via several methods, including molecular beam epitaxy (MBE),^{18–20} metalorganic chemical vapor deposition (MOCVD),^{21–23} halide vapor-phase epitaxy (HVPE),^{24–27} and low-pressure chemical vapor deposition (LPCVD).^{28–30} Each growth method is associated with different challenges. For example, MBE of β -Ga₂O₃ has involved difficulties in n-type doping control at low concentrations. Furthermore, although HVPE and LPCVD epitaxy are suitable for growing thick films for vertical power devices, it is difficult to grow heterostructures or achieve precise control

of epilayers in the nanometer range using these techniques. MOCVD epitaxy is an industrially preferred growth method for semiconductor device technologies. However, substantial efforts are still required to develop high-quality β -Ga₂O₃ and AlGaO/GaO heterostructures. A comprehensive understanding of the fundamental properties of these materials and structures remains elusive.

In this study, we investigated the key MOCVD growth parameters in an effort to achieve high-purity and high-quality β-Ga₂O₃ thin films grown on Fe-doped semi-insulating (010) Ga₂O₃ substrates. Material characterization via scanning electron microscopy (SEM), atomic force microscopy (AFM), secondary-ion mass spectroscopy (SIMS), and X-ray diffraction demonstrated the successful formation of high-quality MOCVD β-Ga₂O₃ thin films. The temperature-dependent charge transport properties were used as a sensitive probe for the electronic properties of the obtained films. Detailed scattering mechanisms and the two-donor model were used to extract the fundamental material parameters, such as the two donor concentrations, their corresponding activation energies, and the compensation concentration.

Si-doped β-Ga₂O₃ thin films were grown on (010)-oriented Fe-doped semi-insulating native substrates (Novel Crystal Technology, Inc.) via MOCVD. Triethylgallium and O₂ were used as the precursors and Ar was used as the carrier gas. Silicon was introduced into the reactor as a dopant via a flow of silane (SiH₄) balanced with Ar. β-Ga₂O₃ thin films with controllable n-type doping concentrations were achieved by tuning the flow rate of SiH₄. Key MOCVD growth parameters, including the growth temperature, VI/III ratio, and chamber pressure, were varied to achieve high-quality β-Ga₂O₃ thin films.

Field emission scanning electron microscopy (FESEM, FEI Helios 600) was used to characterize the surface morphology of the β-Ga₂O₃ thin films with both large field of view and

high resolution. The homoepitaxial β -Ga₂O₃ thin-film growth rate was estimated by measuring the film thickness of co-loaded heteroepitaxial β -Ga₂O₃ films grown on c-sapphire substrates. The surface roughness of the β -Ga₂O₃ films was examined using AFM (Bruker AXS Dimension Icon). The impurity compositions of the epilayers were quantitatively characterized using calibrated SIMS depth profiles. The room-temperature net carrier concentration and corresponding electron Hall mobility were measured using an Ecopia HMS-3000 Hall measurement system. Temperature-dependent Hall measurements were acquired using a Lake Shore 8400 Series Hall effect system. For the Hall measurements, 30/200 nm Ti/Au ohmic contacts were sputtered on the four corners of each sample.

The growth temperature, VI/III ratio, and growth pressure, which are important parameters influencing film growth during MOCVD, were investigated systematically. Various material properties, including epilayer growth rates, doping concentrations, and electron mobilities, were measured to evaluate the effects of the growth parameters on the material properties.

The growth temperature was varied between 800 and 880 °C. Within this temperature range, the films exhibited similar growth rates and Si incorporation. Room-temperature van der Pauw Hall measurements also revealed similar electron mobilities for films grown in this temperature range. However, SEM examination of the surface morphology showed that the β-Ga₂O₃ surface tended to become rougher at lower growth temperatures, and visible macroscopic dents were observed. In contrast, a uniform and smooth surface morphology was observed at a growth temperature of 880 °C. Higher growth temperatures induce the surface diffusion of adatoms with high mobilities, thereby promoting smooth epi-film formation.

Figure 1(a) shows the surface morphology of a representative β -Ga₂O₃ film grown at 880 °C with a large field of view. The surface was clean and uniform across the entire sample (15 mm × 10 mm). From a tilted viewing angle (45° relative to the incident electron beam) with higher magnification (Fig. 1(b)), examination of the surface morphology revealed the presence of elongated grains. The AFM image of the same sample revealed that the groove structures were along the (001) crystal orientation with a root-mean-square roughness of 1.7 nm (Fig. 1(c)). The surface morphology of β -Ga₂O₃ is known to be strongly dependent on the growth temperature, which is an important parameter influencing adatom diffusion at the growth surface. For example, β -Ga₂O₃ thin films grown via MBE at 500–650 °C exhibited smooth surfaces, whereas those grown at >700 °C exhibited step bunching along the [100] orientation, the severity of which increased with increasing temperature.²⁰ LPCVD β -Ga₂O₃ thin films are typically grown at 850–1050 °C, and their surfaces have been reported to exhibit prominent (001)-oriented step bunching.²⁹

The influence of the VI/III ratio on the MOCVD growth of β -Ga₂O₃ was also investigated. Variation of the VI/III ratio between 930 and 1350 was achieved by tuning the O₂ flow rate at a fixed triethylgallium flow rate. High-quality β -Ga₂O₃ thin films with high electron mobilities were obtained throughout this range of VI/III ratios. The film growth rate within this range remained similar at 0.65–0.7 μ m/h, as it was primarily limited by the triethylgallium flow rate. The Si dopant incorporation efficiency (n = 1.5–2×10¹⁷ cm⁻³) and electron mobility (~ 140 cm²/V·s at room temperature) also remained similar within this VI/III ratio range. These results indicate that high-quality β -Ga₂O₃ thin films can be grown over a wide range of MOCVD growth conditions.

Selected representative MOCVD-grown β-Ga₂O₃ thin films were characterized using SIMS depth profiles to quantitatively probe the impurity concentrations. As shown in Fig. 2, the doped Si concentration was uniform ($\sim 3 \times 10^{17}$ cm⁻³) across the depth of the epilayer with a thickness of 1.25 µm, except for a noticeable peak at the epilayer/substrate interface, which has been frequently observed in previous studies.^{22,30} This Si peak may be attributable to surface contamination/residue from substrate processing, although further research would be required to confirm the mechanism. Detectable Fe impurities were observed in the first 200 nm of the epilayer, which can be ascribed to diffusion from the Fe-doped Ga₂O₃ substrate. At depths further from the epilayer/substrate interface, the Fe impurity level was below the detection limit of 1×10¹⁵ cm⁻³. The levels of other impurities, namely, hydrogen (H), carbon (C), and chlorine (Cl), were all below the corresponding detection limits of the instrument: H $(2\times10^{16} \text{ cm}^{-3})$, C (2×10¹⁶ cm⁻³), and Cl (5×10¹⁴ cm⁻³). High-purity β-Ga₂O₃ thin films were therefore achieved using our MOCVD epitaxy process. This can be further verified by low-temperature Hall measurements as discussed later, which is a sensitive characterization technique for probing ionized impurity scattering.

The growth pressure is a key parameter influencing the growth of β -Ga₂O₃ thin films during MOCVD. Table I presents a comparison of the properties of five β -Ga₂O₃ samples grown at various chamber pressures ranging from 20 to 100 Torr. The films were grown at a fixed growth temperature of 880 °C and VI/III ratio of 1150. The film growth rate decreased monotonically with increasing chamber pressure, which could be attributable to (i) a decrease in precursor diffusion from the gas phase to the growth surface, and (ii) an increase in the gas-phase reaction of the precursors. This decrease in growth rate with increasing chamber pressure led to an increase in the Si doping concentration from 1.4×10^{16} to 3.9×10^{16} cm⁻³, as shown in Table I.

Within the range of growth pressures studied, a record-high room-temperature mobility of 184 cm²/V·s was observed for the sample grown at 60 Torr (sample #3) with a doping concentration of 2.5×10^{16} cm⁻³.

Figure 3 shows a plot of the room-temperature mobility versus carrier concentration for four MOCVD-grown β -Ga₂O₃ films alongside previously reported state-of-the-art films. 19,22,23,26,27,30,31 The four films exhibited higher room-temperature mobilities at various carrier concentrations than the previously reported results. The room-temperature mobilities of our MOCVD-grown β -Ga₂O₃ films approach the predicted theoretical limit of approximately 200 cm²/V·s. 32 For pure β -Ga₂O₃ materials, the room-temperature mobility is limited by polar phonon scattering owing to the strong ionic Ga–O bonding. 32,33 As the doping concentration increases, the increased ionized impurity scattering and neutral impurity scattering become dominant factors limiting the room-temperature mobility. 34

A selected representative sample was characterized via temperature-dependent Hall measurements in the van der Pauw configuration to probe the donor activation energy and compensation concentration, as shown in Fig. 4. Ti (30 nm)/Au (200 nm) ohmic contacts were deposited on the corners of the sample and used to perform temperature-dependent Hall measurements after wire bonding. The temperature was varied from 32 to 300 K. The measured room-temperature electron mobility was 160 cm²/V·s with a carrier concentration of 2.75×10¹⁶ cm⁻³. A peak mobility as high as 4984 cm²/V·s was achieved at a temperature of 45 K, which represents a new record of peak electron mobility for β-Ga₂O₃ epitaxy. The recently reported room temperature and peak electron mobilities for an MOCVD-grown unintentionally doped β-Ga₂O₃ film were 176 cm²/V·s and 3481 cm²/V·s, respectively, with a room-temperature net carrier concentration of 7.4×10¹⁵ cm⁻³.²³

The higher peak electron mobility occurring at lower temperature indicates a lower compensation concentration (N_A) in our MOCVD-grown β -Ga₂O₃ samples. We next performed mobility calculations by considering various scattering mechanisms, including polar optical phonon (μ_{POP}) scattering, acoustic deformation potential (μ_{ADP}) scattering, and ionized impurity (μ_{II}) and neutral impurity (μ_{NI}) scattering.

The total carrier mobility (μ_{mob}) can be calculated according to Matthiessen's rule:

$$\tau_{\text{total}}^{-1} = \tau_{\text{POP}}^{-1} + \tau_{\text{II}}^{-1} + \tau_{\text{NI}}^{-1} + \tau_{\text{ADP}}^{-1}$$

$$\mu_{\text{mob}} = \frac{q\tau_{\text{total}}}{m^*}$$

where τ_{total} is the total relaxation lifetime of the carriers, τ_{POP} , τ_{II} , τ_{NI} , and τ_{ADP} are the relaxation times for each scattering mechanism, and m^* is the effective electron mass. The relaxation time for each scattering mechanism was calculated as described previously.^{32,35} The parameters used in the analysis are listed in Table II.^{2,32,36–38} Note that the phonon energy of 47 meV was a fitted value obtained from our experimental data.

Our analysis indicated that the two-donor model^{23,39} is appropriate for fitting both the temperature-dependent mobility and carrier concentration data. The charge neutrality equation can be expressed as follows:

$$n + N_{A} = \frac{N_{d1}}{1 + 2e^{-(E_{d1} - E_{F})}/k_{B}T} + \frac{N_{d2}}{1 + 2e^{-(E_{d2} - E_{F})}/k_{B}T}$$

where N_A is the concentration of acceptors acting as compensators, N_{d1} and N_{d2} are the concentrations of the two donors, and E_{d1} and E_{d2} are the corresponding activation energies.

As listed in Table III, fitting of the temperature-dependent carrier mobility and carrier concentration data afforded a low compensation concentration of $N_A = 9.4 \times 10^{14}$ cm⁻³, as expected from the high peak mobility at low temperature. The primary donor state was located at an activation energy of $E_{d1} = 34.9$ meV and a donor concentration of $N_{d1} \approx 2.7 \times 10^{16}$ cm⁻³, whereas the secondary donor state was located at $E_{d2} = 120$ meV and a donor concentration of $N_{d2} \approx 5 \times 10^{15}$ cm⁻³. DFT calculations indicate that Si prefers the tetrahedrally coordinated Ga(I) site, in which it is the primary shallow donor.² Possible origins of the secondary donor state at 120 meV could include antisites, interstitials, impurities such as hydrogen, or Si on the octahedrally coordinated Ga(II) site.³⁹

The low compensation concentration of the MOCVD-grown β -Ga₂O₃ films is expected to permit controllable n-type doping as low as low-mid 10^{15} cm⁻³, which is critical for developing high-performance lateral and vertical power devices with high critical fields. To attain a comprehensive understanding of the MOCVD-grown β -Ga₂O₃ thin films, characterization of the defects using techniques such as scanning transmission electron microscopy and deep-level transient spectroscopy or deep-level optical spectroscopy is necessary.

In summary, Si-doped homoepitaxial (010) β -Ga₂O₃ thin films with high purity and high quality have been grown using MOCVD and found to exhibit record-high carrier mobilities of 184 cm²/V·s at room temperature and 4984 cm²/V·s at 45 K for samples with room-temperature carrier concentrations of 2.5×10^{16} and 2.75×10^{16} cm⁻³, respectively. The extracted compensation concentration was as low at 9.4×10^{14} cm⁻³, which is critical for controllable tuning of the doping concentration as low as low-mid 10^{15} cm⁻³. The excellent electrical transport properties of the asgrown β -Ga₂O₃ films, the smooth surface morphology at the atomic level, and the reasonable

growth rate of approximately 1 μ m/h are key factors for developing high-performance power electronic devices with a high breakdown field and low on resistance.

ACKNOWLEDGMENTS

The authors acknowledge the funding support from the Air Force Office of Scientific Research FA9550-18-1-0479 (AFOSR, Dr. Ali Sayir) and the National Science Foundation (1810041). ZF also thanks Dr. Yuewei Zhang for discussions regarding data fitting of temperature-dependent Hall measurements.

REFERENCES

- H. Peelaers and C. G. Van de Walle, Phys. Status Solidi B **252**, 828 (2015).
- ² J. B. Varley, J. R. Weber, A. Janotti, and C. G. Van de Walle, Appl. Phys. Lett. **97**, 142106 (2010).
- M. Higashiwaki, K. Sasaki, A. Kuramata, T. Masui, and S. Yamakoshi, Appl. Phys. Lett. 100, 013504 (2012).
- ⁴ T. Oshima, T. Okuno, N. Arai, N. Suzuki, S. Ohira, and S. Fujita, Appl. Phys. Express 1, 011202 (2008).
- ⁵ B. J. Baliga, J. Appl. Phys. **53**, 1759 (1982).
- ⁶ N. Ueda, H. Hosono, R. Waseda, and H. Kawazoe, Appl. Phys. Lett. **71**, 933 (1997).
- E. G. Villora, K. Shimamura, Y. Yoshikawa, K. Aoki, and N. Ichinose, J. Cryst. Growth **270**, 420 (2004).
- S. Ohira, N. Suzuki, N. Arai, M. Tanaka, T. Sugawara, K. Nakajima, and T. Shishido, Thin Solid Films **516**, 5763 (2008).
- N. Suzuki, S. Ohira, M. Tanaka, T. Sugawara, K. Nakajima, and T. Shishido, Phys. Status Solidi C 4, 2310 (2007).
- ¹⁰ Y. Tomm, P. Reiche, D. Klimm, and T. Fukuda, J. Cryst. Growth **220**, 510 (2000).
- ¹¹ Z. Galazka, R. Uecker, K. Irmscher, M. Albrecht, D. Klimm, M. Pietsch, M. Brützam, R. Bertram, S. Ganschow, and R. Fornari, Cryst. Res. Technol. **45**, 1229 (2010).
- ¹² Z. Galazka, R. Uecker, D. Klimm, K. Irmscher, M. Naumann, M. Pietsch, A. Kwasniewski, R. Bertram, S. Ganschow, and M. Bickermann, ECS J. Solid State Sci. Technol. 6, Q3007 (2017).
- H. Aida, K. Nishiguchi, H. Takeda, N. Aota, K. Sunakawa, and Y. Yaguchi, Jpn. J. Appl. Phys. 47, 8506 (2008).

- ¹⁴ A. Kuramata, K. Koshi, S. Watanabe, Y. Yamaoka, T. Masui, and S. Yamakoshi, Jpn. J. Appl. Phys. **55**, 12 (2016).
- J. Yang, F. Ren, M. Tadjer, S. J. Pearton, and A. Kuramata, ECS J. Solid State Sci. Technol. 7, Q92 (2018).
- M. H. Wong, K. Sasaki, A. Kuramata, S. Yamakoshi, and M. Higashiwaki, IEEE Electron Device Lett. **37**, 212 (2016).
- Y. Zhang, A. Neal, Z. Xia, C. Joishi, J. Johnson, Y. Zheng, S. Bajaj, M. Brenner, D. Dorsey, K. Chabak, G. Jessen, J. Hwang, S. Mou, J. Heremans, and S. Rajan, Appl. Phys. Lett. 112, 173502 (2018).
- ¹⁸ T. Oshima, N. Arai, N. Suzuki, S. Ohira, and S. Fujita, Thin Solid Films **516**, 5768 (2008).
- ¹⁹ K. Sasaki, A. Kuramata, T. Masui, E. G. Villora, K. Shimamura, and S. Yamakoshi, Appl. Phys. Express **5**, 035502 (2012).
- ²⁰ K. Sasaki, M. Higashiwaki, A. Kuramata, T. Masui, and S. Yamakoshi, J. Cryst. Growth **392**, 30 (2014).
- ²¹ G. Wagner, M. Baldini, D. Gogova, M. Schmidbauer, R. Schewski, M. Albrecht, Z. Galazka, D. Klimm, and R. Fornari, Phys. Status Solidi A **211**, 27 (2014).
- M. Baldini, M. Albrecht, A. Fiedler, K. Irmscher, R. Schewski, and G. Wagner, ECS J. Solid State Sci. Technol. **6**, Q3040 (2017).
- ²³ Y. Zhang, F. Alema, A. Mauze, O. S. Koksaldi, R. Miller, A. Osinsky, and J. S. Speck, APL Mater. 7, 022506 (2019).
- ²⁴ K. Nomura, K. Goto, R. Togashi, H. Murakami, Y. Kumagai, A. Kuramata, S. Yamakoshi, and A. Koukitu, J. Cryst. Growth **405**, 19 (2014).
- ²⁵ Y. Oshima, E.G. Villora, and K. Shimamura, J. Cryst. Growth **410**, 53 (2015).
- ²⁶ K. Goto, K. Konishi, H, Murakami, Y, Kumagai, B. Monemar, M. Higashiwaki, A. Kuramata, and S. Yamakoshi, Thin Solid Films **666**, 182 (2018).
- ²⁷ J. H. Leach, K. Udwary, J. Rumsey, G. Dodson, H. Splawn, and K. R. Evans, APL Mater. 7, 022504 (2019).
- ²⁸ S. Rafique, L. Han, A. T. Neal, S. Mou, M. J. Tadjer, R. H. French, and H. Zhao, Appl. Phys. Lett. **109**, 132103 (2016).
- ²⁹ S. Rafique, L. Han, M. J. Tadjer, J. A. Freitas Jr., N. A. Mahadik, and H. Zhao, Appl. Phys. Lett. **108**, 182105 (2016).
- S. Rafique, M. R. Karim, J. M. Johnson, J. Hwang, and H. Zhao, Appl. Phys. Lett. 112, 052104 (2018).
- E. Ahmadi, O. S. Koksaldi, S. W. Kaun, Y. Oshima, D. B. Short, U. K. Mishra, and J. S. Speck, Appl. Phys. Express 10, 041102 (2017).
- N. Ma, N. Tanen, A. Verma, Z. Guo, T. Luo, H. Xing, and D. Jena, Appl. Phys. Lett. 109, 212101 (2016).
- ³³ H. He, M. A. Blanco, and R. Pandey, Appl. Phys. Lett. **88**, 261904 (2006).
- ³⁴ Y. Kang, K. Krishnaswamy, H. Peelaers, and C. G. Van de Walle, J. Phys.: Condens. Matter **29**, 234001 (2017).

- A. T. Neal, S. Mou, S. Rafique, H. Zhao, E. Ahmadi, J. S. Speck, K. T. Stevens, J. D. Blevins, D. B. Thomson, N. Moser, K. D. Chabak, and G. H. Jessen, Appl. Phys. Lett. 113, 062101 (2018).
- ³⁶ A. Parisini and R. Fornari, Semicond. Sci. Technol. **31**, 035023 (2016).
- ³⁷ Z. Guo, A. Verma, X. F. Wu, F. Y. Sun, A. Hickman, T. Masui, A. Kuramata, M. Higashiwaki, D. Jena, and T. F. Luo, Appl. Phys. Lett. **106**, 111909 (2015).
- M. Passlack, N. E. J. Hunt, E. F. Schubert, G. J. Zydzik, M. Hong, J. P. Mannaerts, R. L. Opila, and R. J. Fischer, Appl. Phys. Lett. **64**, 2715 (1994).
- A. T. Neal, S. Mou, R. Lopez, J. V. Li, D. B. Thomson, K. D. Chabak, and G. H. Jessen, Sci. Rep. 7, 13218 (2017).

Table Caption

Table I. Comparison of five MOCVD grown (010) β-Ga₂O₃ samples with different chamber pressure from 20 up to 100 Torr. The growth rate, room temperature carrier concentration, and Hall mobility were listed for comparison.

Table II. Material parameters of β-Ga₂O₃ used for mobility calculations.

Table III. Extracted donor parameters and acceptor concentration from the fitting to the temperature dependent Hall charge concentration data.

Figure Caption

Figure 1. (a-b) Top view FESEM images of MOCVD grown (010) β-Ga₂O₃ homoepitaxial thin film with large field of view (a), and high magnification (b). Viewing angle of SEM was 45° tilted against surface. (c) AFM image for the same β-Ga₂O₃ sample.

Figure 2. SIMS depth profile of impurities (Si, C, H, Cl, and Fe) in MOCVD grown (010) β-Ga₂O₃ homoepitaxial thin film. This sample shows net carrier concentration of 1.01×10^{17} cm⁻³ and room temperature mobility of 152 cm²/V·s from Hall measurement.

Figure 3. Results from this work as compared to state-of-the-art: room temperature carrier mobility vs. carrier concentration for (010) β -Ga₂O₃ films.

Figure 4. (a) Measured and calculated temperature dependent carrier mobility as a function of temperature. Dots represent the measurement data while colored dash lines represent mobility values calculated for each scattering mechanism. Black dash line represents the total mobility as a function of temperature, calculated by the Matthiessen's rule. (b) Measured carrier concentration as a function of 1000/T and the calculated concentration from the two-donor model. Dots represent experimental data and dash line is obtained from calculation.

Table I

Sample	Chamber pressure	Growth rate	Doping concentration	Mobility
	(Torr)	$(\mu m/h)$	(cm^{-3})	$(cm^2/V \cdot s)$
#1	20	0.82	1.4×10^{16}	168
#2	40	0.75	1.8×10^{16}	171
#3	60	0.71	2.5×10^{16}	184
#4	80	0.62	3.6×10^{16}	158
#5	100	0.53	3.9×10^{16}	162

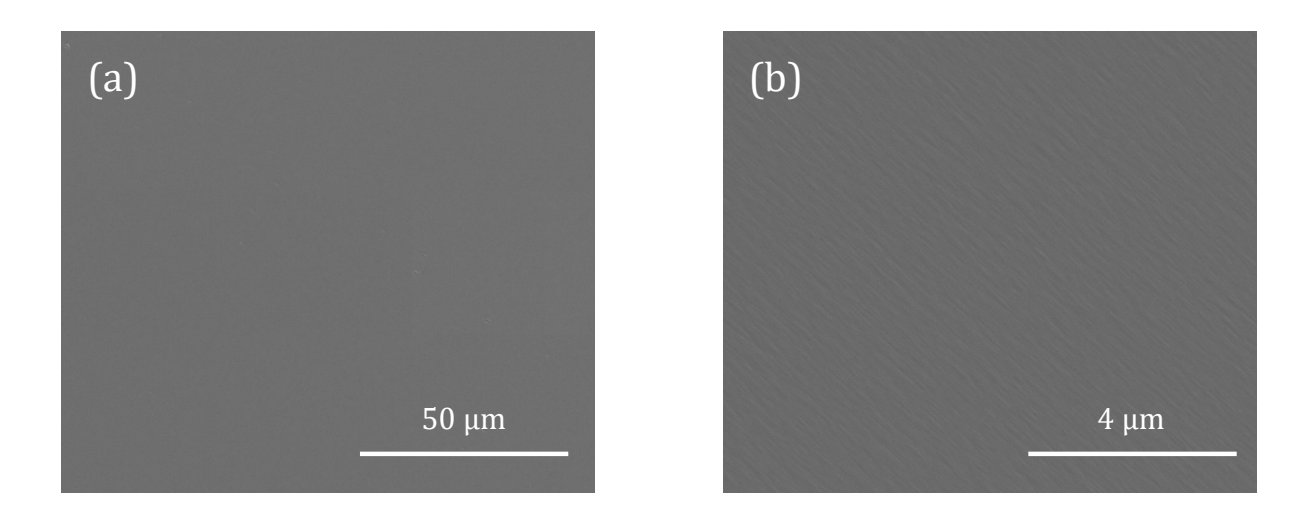
Table II

Calculation parameter	Symbol	Value
Phonon energy (meV)	$\hbar\omega_0$	47 (fitted)
Dielectric constant	$\mathcal{E}_{ extsf{S}}$	10.2
High-frequency dielectric constant	$arepsilon_0$	3.6
Electron effective mass (m_0)	m^*	0.313
Acoustic deformation potential (eV)	$E_{ m ADP}$	6.9 eV
Mass density (kg/m³)	ho	5.88×10^{3}
Sound velocity (m/s)	$v_{ m s}$	6.8×10^3

Table III

$N_{\rm d1}~(\rm cm^{-3})$	$E_{\rm d1}~({\rm meV})$	$N_{\rm d2}~({\rm cm}^{-3})$	$E_{\rm d2}~({\rm meV})$	$N_{\rm A}~({\rm cm}^{-3})$
2.7×10^{16}	34.9	5.0×10^{15}	120	9.4×10^{14}

Figure 1.



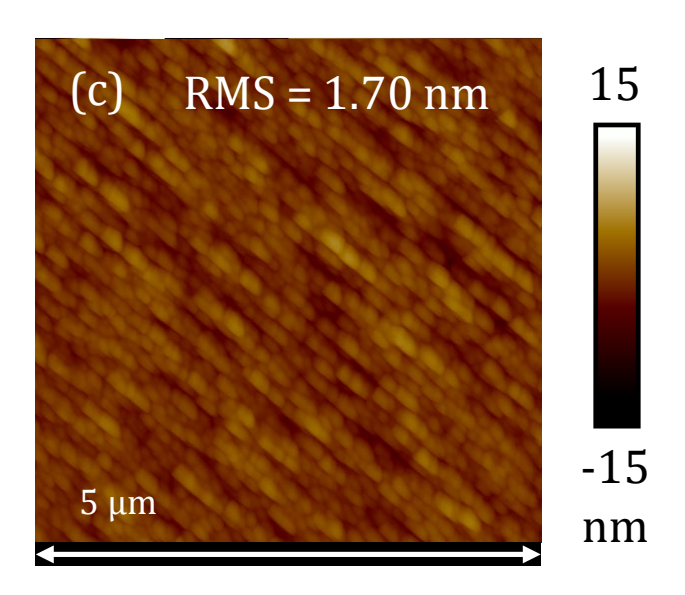


Figure 2.

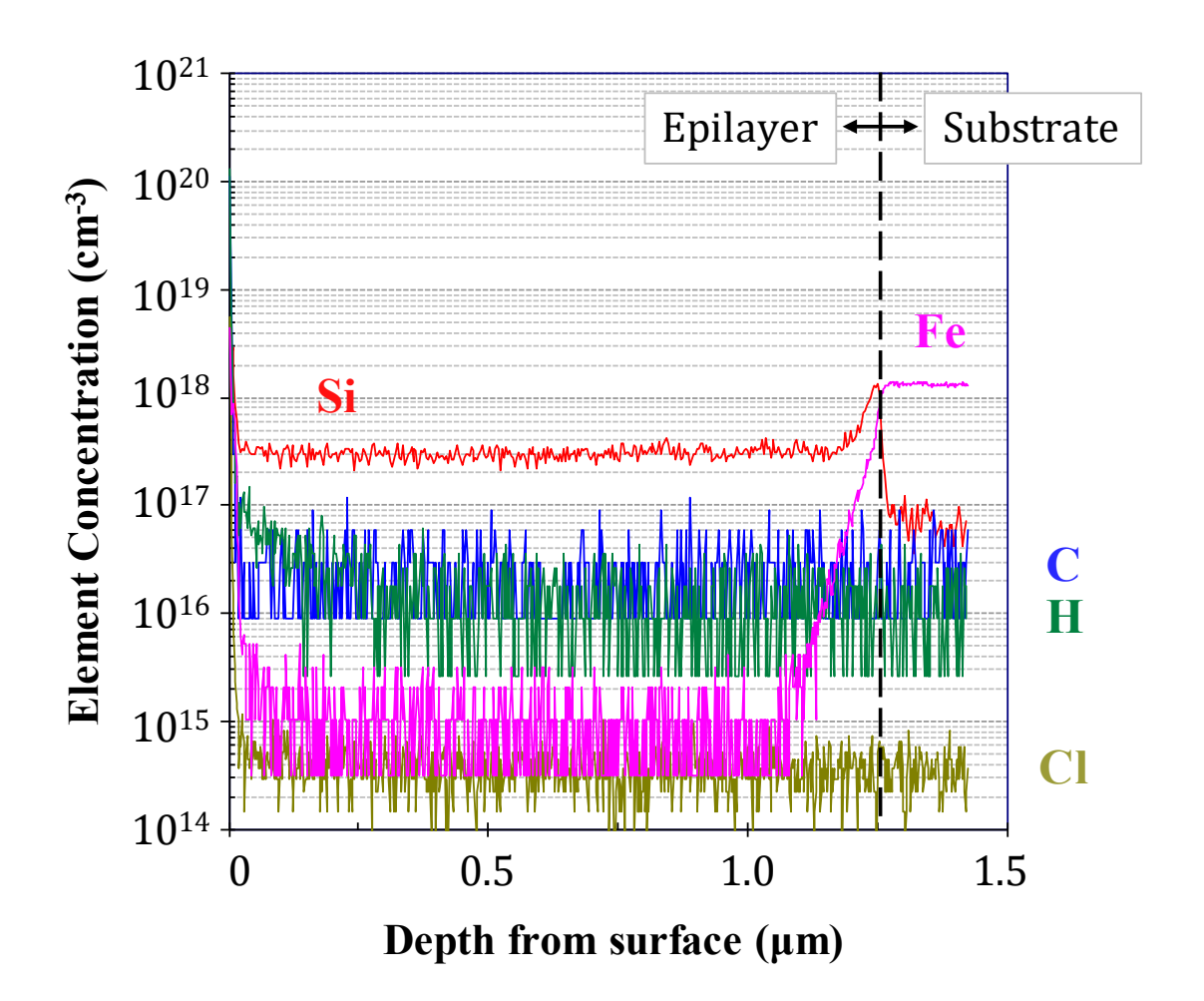


Figure 3.

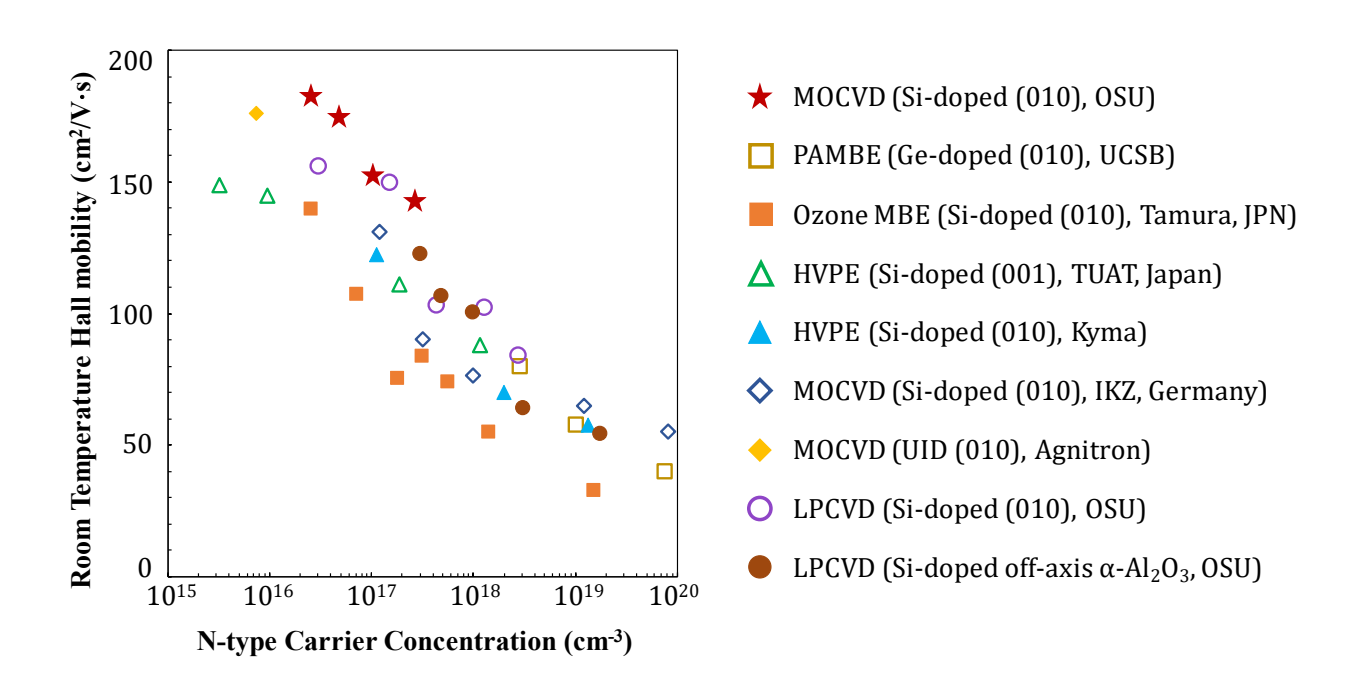


Figure 4.

